

Radiation-Balanced Silica Fiber Amplifier

Jennifer M. Knall,^{1,*} Magnus Engholm,² Tommy Boilard,³ Martin Bernier,³ and Michel J. F. Digonnet¹¹*Edward L. Ginzton Laboratory, Stanford University, Stanford, California 94305, USA*²*Division of Electronics Design, Mid Sweden University, SE-85170 Sundsvall, Sweden*³*Centre d'optique, photonique et laser (COPL), Université Laval, Québec, Canada QC G1V 0A6*

(Received 8 February 2021; accepted 7 June 2021; published 2 July 2021)

We report what we believe to be the first radiation-balanced fiber amplifier—a device that provides optical gain while experiencing no temperature rise. The gain medium is a silica fiber with a 21- μm -diameter core highly doped with Yb^{3+} (2.52 wt. %) and codoped with 2.00 wt. % Al to reduce concentration quenching. The amplifier is core pumped with 1040-nm light to create anti-Stokes fluorescence cooling and gain in the core at 1064 nm. Using a custom slow-light fiber Bragg grating sensor with mK resolution, temperature measurements are performed at multiple locations along the amplifier fiber. A 4.35-m fiber pumped with 2.62 W produced 17 dB of gain, while the average fiber temperature remained slightly below room temperature. This advancement is a fundamental step toward the creation of ultrastable lasers necessary to many applications, especially low-noise sensing and high-precision metrology.

DOI: 10.1103/PhysRevLett.127.013903

Since the first rare-earth-doped fiber laser was fabricated using modified chemical vapor deposition (MCVD) in 1985 [1], tremendous advancements have been made in fiber laser technology. Fiber lasers now produce coherent emission ranging from the UV to the mid-IR, in continuous-wave, Q -switched, and mode-locked outputs. They can exhibit extremely stable single-frequency emission with linewidths as narrow as a few kilohertz [2], and they can be scaled up to 10 kW in a single-mode output [3], making them the brightest humanmade light sources. One of the main challenges limiting further power scaling and improvements in temporal and spatial quality is the internal heat introduced by the laser's quantum defect. The quantum defect is the energy difference between the pump and laser photons, and it is converted into heat through nonradiative relaxation. In Yb^{3+} , which has one of the smallest quantum defects, this energy difference is only 4%–8% of the pump photon energy [4]. Yet this is enough that even a relatively low-power 1-W Yb -doped laser can experience several degrees of heating [5]. Temperature variations induce instabilities in the laser frequency, which cause linewidth broadening and an increase in frequency noise [6]. In high-power lasers, they also limit the output power through transverse mode instability [7]. In the most extreme case, heating will fracture or melt the fiber.

Currently, thermal effects are mitigated by either water cooling or thermoelectric cooling. While these solutions are comparatively energy efficient, water-cooled systems are prone to leaking, add significant bulk to the laser, and induce vibrations that degrade the spectral and spatial beam quality. Thermoelectric coolers are generally vibration-free, but they tend to cool the fiber asymmetrically, which creates undesirable thermal gradients. Optical parametric

oscillators and amplifiers are also a viable solution, as they do not exhibit a quantum defect, but they represent a small minority of all lasers and amplifiers.

First proposed in 1999, heat mitigation through anti-Stokes fluorescence (ASF) cooling has emerged as a promising potential solution [8,9]. Cooling is induced when a gain medium is optically or electronically pumped at an energy lower than the average energy of the radially escaping fluorescence [10] (calculated from the emission spectrum). Energy is extracted in three main steps. First, the pump excites electrons from a higher sublevel of the ground manifold of the laser ion to a low-lying sublevel of the upper manifold. The Maxwell-Boltzmann law stipulates that the electrons must be distributed exponentially within all levels of the upper manifold. Therefore, the low-lying electrons then acquire energy from the host's phonon bath and redistribute themselves to higher sublevels until this distribution is satisfied. Finally, this extra energy (as well as the pump energy) is carried out of the sample when the electrons relax radiatively to the ground manifold and emit fluorescence with a higher average photon energy than the pump. This fluorescence escapes radially from the gain medium. ASF cooling is closely related to a number of common techniques used to cool atoms with a laser, which rely on the absorption and reemission of light to alter the momentum of an atom. ASF cooling adds minimal bulk to the laser and no moving parts. It eliminates harmful vibrations, prolongs the lifetime of the laser, and minimizes maintenance time and cost. One of the main downsides is that it requires a pump with a longer wavelength. This decreases the pump absorption strength and, to compensate, increases the required fiber length. Also, the efficiency of ASF cooling is relatively low, so higher pump powers are required.

Since the heat extracted per electron is the small energy difference between the pump and fluorescence photons, ASF cooling extracts relatively small amounts of energy per unit volume [10]. Therefore, any number of extraneous exothermic effects can either partially negate or overwhelm the cooling. The most common mechanisms are residual absorption of pump or fluorescence photons by impurities in the gain medium [11] and concentration quenching [12]. To achieve useful ASF cooling, it is paramount to select a combination of rare-earth ion and host composition that minimizes these two deleterious effects, especially the latter. Until recently, this limitation restricted ASF cooling to exotic crystals or fluorides with low quenching and absorptive loss, and experiments were often performed in a vacuum to minimize the heat load from air convection. The only two ASF-cooled radiation-balanced lasers reported to date used highly doped Yb:YLF crystals [9,13]. In Ref. [9], a 3×120 mm rod was pumped at 1030 nm to simultaneously induce lasing at 1050 nm and ASF cooling. Since the extracted heat is proportional to the optically excited doped area, which is relatively large in a bulk laser, the extracted heat was significant, and the laser was able to output 80 W while maintaining zero average temperature change along the crystal. Since then, several theoretical papers have presented models for radiation-balanced operation in semiconductor [14] and fiber [15–17] lasers and in fiber amplifiers [18,19], but none of these devices have been demonstrated experimentally. For fiber devices, this is partly due to the limited heat that can be removed from a fiber because of the small volume of the doped core [20]. Also, until recently, cooling in fibers had been primarily limited to fluorides [21–23], the only fiber host known to offer both high quenching-free rare-earth concentrations and low residual absorptive loss. Given the overwhelmingly commercial dominance of silica in fiber lasers and amplifiers, it was paramount to achieve cooling in this host.

Toward the end of 2019, this situation changed drastically with breakthrough work that demonstrated the first cooling of a Yb-doped silica fiber [24] and of a Yb-doped fiber preform [25]. A few months later, significantly more cooling was reported in a silica fiber with an improved composition [26] and in a silica preform placed in vacuum [27]. Temperature changes as large as -70 mK were measured in the fiber at atmospheric pressure [26], and up to -6 K was measured in the preform [27]. The work of Refs. [25–27] demonstrated that silica fibers with the right composition and fabrication method can be cooled with efficiencies close to those of fluoride fibers [23].

Capitalizing on this innovation, we report here the first internally cooled fiber amplifier. The main objective of this work is to demonstrate that the seemingly small amount of cooling exhibited in fibers is sufficient to negate the heating induced by significant amplification of a seed signal. This work proves that it is possible to observe simultaneous cooling and amplification in a core-pumped Yb-doped

fiber, ultimately resulting in the first fiber device that demonstrates gain without heating. In addition, it does so in a silica fiber, the workhorse of fiber lasers and amplifiers, an accomplishment that opens the door to a wealth of new internally cooled fiber devices.

In the limit of negligible absorptive loss, the maximum heat that can be extracted per unit length from a fiber doped with a two-level laser ion is quantified by [20]

$$\left(\frac{dQ}{dt}\right)_{\max} = \left(\frac{\tau_{\text{rad}}}{\tau(N_0)}hv_p - h\langle v_f \rangle\right) \frac{\sigma_p^a}{\sigma_p^a + \sigma_p^e} \frac{\pi a^2}{\tau_{\text{rad}}} N_0, \quad (1)$$

where N_0 is the ion concentration, a is the radius of the doped core, τ_{rad} is the radiative lifetime of the ions, hv_p is the energy of the pump photon, $h\langle v_f \rangle$ is the average energy of the fluorescence photons, and σ_p^a and σ_p^e are the pump absorption and emission cross sections of the ions, respectively. The lifetime $\tau(N_0)$ is the total concentration-dependent upper-state lifetime, including quenching-induced relaxation. It depends on the degree of concentration quenching according to [12]

$$\tau(N_0) = \frac{\tau_0}{1 + \frac{9}{2\pi} \left(\frac{N_0}{N_c}\right)^2}, \quad (2)$$

where τ_0 is the total lifetime at sufficiently low Yb concentrations and N_c is the critical concentration. In silica, the upper laser state of Yb^{3+} is almost purely radiative, and τ_0 is essentially equal to the radiative lifetime τ_{rad} . The fiber cools when the term in parentheses in Eq. (1) is negative. This occurs when the pump photon energy is lower than the average energy of the fluorescence photons *and* quenching is negligible [$\tau(N_0) \approx \tau_{\text{rad}}$]. From Eq. (1), maximum ASF cooling is achieved with a large doped area, a short radiative lifetime, and a large energy difference between the pump and the fluorescence photons. There is also an optimum Yb concentration due to two competing effects—increasing N_0 increases the number of heat engines (greater cooling), but it also decreases $\tau(N_0)$ [see Eq. (2)] (less cooling). Since the optimum Yb concentration increases with N_c , for significant cooling it is paramount to develop glass with compositions and thermal histories that result in high N_c values.

With these considerations in mind, the amplifier was constructed with the best performing silica fiber reported in Ref. [26]. Its core (21- μm diameter) is codoped with 2.0 wt. % Al to reduce concentration quenching [28], allowing the core to be highly doped with 2.52 wt. % Yb (1.93×10^{26} Yb ions/ m^3). From the fiber's measured emission spectrum, the mean fluorescence wavelength was found to be relatively low (1003.9 nm), corresponding to a large average energy difference between the fluorescence and the 1040-nm pump photons [see Eq. (1)]. The relatively short upper-state lifetime of the Yb ions (765 μs) is also beneficial to cooling. The preform was fabricated using

TABLE I. Yb-doped fiber parameters.

Fiber parameter	Parameter value
Yb ³⁺ concentration (N_0)	2.52 wt. % Yb
Al ⁻ concentration (N_{Al})	2.00 wt. % Al
Core diameter ($2a$)	21 μm
Numerical aperture (NA)	0.13
Radiative lifetime (τ_{rad})	765 μs
Mean fluorescence wavelength ($\langle\lambda_f\rangle$)	1003.9 nm
Quenching lifetime (τ_q)	38 ms
Critical quenching concentration (N_c)	21.0 wt. % Yb
Absorptive loss (α_{ba})	18 dB/km

MCVD, followed by drawing at about 2000 °C. With a numerical aperture of 0.13, the fiber is slightly multimoded ($V = 8.4$ at 1064 nm). These measured parameter values, along with the parameter values inferred from absorption and temperature measurements (see Supplemental Material [29]), are summarized in Table I.

The fiber was core pumped at 1040 nm to create both cooling and gain at 1064 nm (Fig. 1). A 90/10 fiber splitter combined the pump with the 1064-nm seed. The splitter output that carried 90% of the pump power and 10% of the seed power was spliced to the input of the Yb-doped silica fiber. The other splitter output was used as a tap to measure the power launched into the fiber amplifier. At the amplifier output, a long-pass filter removed the residual pump power and passed the signal to a power meter.

The induced temperature change was measured at seven locations along the Yb-doped fiber using a slow-light fiber Bragg grating (FBG) sensor. Both the index and length of the FBG vary in response to a temperature change, inducing a spectral shift of ~ 10 pm/K (for a silica fiber) that is probed with a 1550-nm tunable laser locked to a resonance peak of the FBG (see Ref. [33] for further details). At each measurement location, an ~ 10 -cm length of the Yb-doped fiber was stripped of its jacket to prevent reabsorption of the radially escaping ASF. The stripped

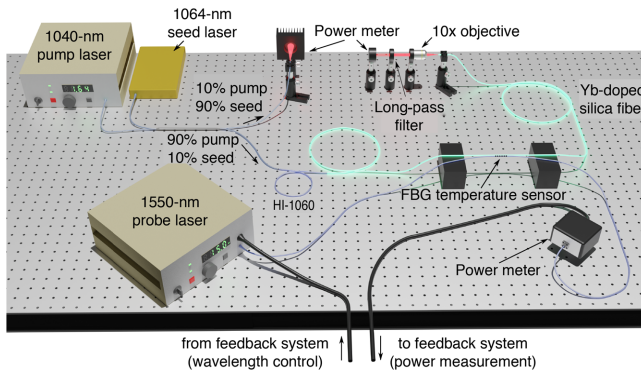


FIG. 1. Schematic of the experimental setup used to measure temperature changes induced in the Yb-doped silica fiber amplifier.

section was placed in contact with the FBG (see Fig. 1), and a small amount of isopropanol was applied between the fibers to hold them together through capillary forces. When the Yb-doped fiber is pumped, its temperature changes and the two fibers quickly (a few seconds) reach thermal equilibrium [5].

Figure 2 shows an exemplary temperature measurement of the fiber amplifier. At time $t = 0$ s, the pump was abruptly turned on, causing the fiber to cool to ~ 130 mK below room temperature. After 15 s, the seed was also turned on, which induced a slight heating (~ 20 mK) to a new steady-state value ~ 110 mK below room temperature. The temperature change of the fiber amplifier was defined as the difference between the average temperature in the first 5 s when both the pump and signal were off and the average temperature in the last 5 s after both had been turned on. Each measurement was repeated three times and averaged.

The first cooled amplifier consisted of a 2.74-m section of Yb-doped silica fiber core pumped with 1.12 W at 1040 nm and seeded with 3 mW at 1064 nm. The temperature changes were measured to be negative at all seven locations (blue squares in Fig. 3), and the small-signal gain was 5.7 dB (11.7 mW of output power at 1064 nm). At low pump powers (below saturation), the Yb ions are insufficiently excited, resulting in low ASF and low extracted heat. At large pump powers (well above saturation), excitation of the Yb ions is saturated and the cooling rate is maximum. While the pump power in excess of the saturation power contributes very little to cooling, it is still absorbed by impurities. The latter process is essentially unsaturable and increases heating in proportion to this additional pump power. These two opposing effects create an optimum pump power that maximizes the extracted heat per unit length. Simulations using a model of ASF cooling in a fiber [20] predict that the optimum pump power for this fiber is 510 mW. In this experiment, the input pump power was 1.12 W, and the residual pump power at the output of the amplifier was only 80.2 mW. It follows that (i) the negative temperature changes are

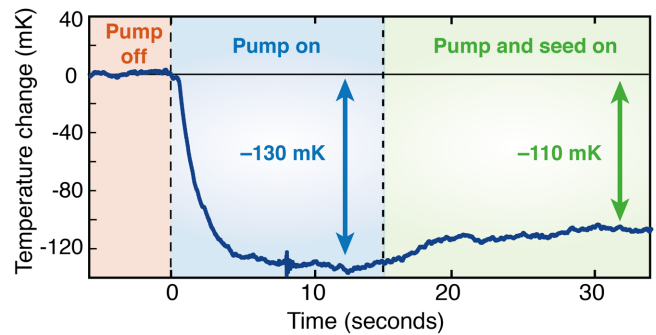


FIG. 2. Measured temporal trace of the temperature change in the Yb-doped silica fiber as the 1040-nm pump (1.64 W) and 1064-nm seed (3 mW) are sequentially launched in the fiber core.

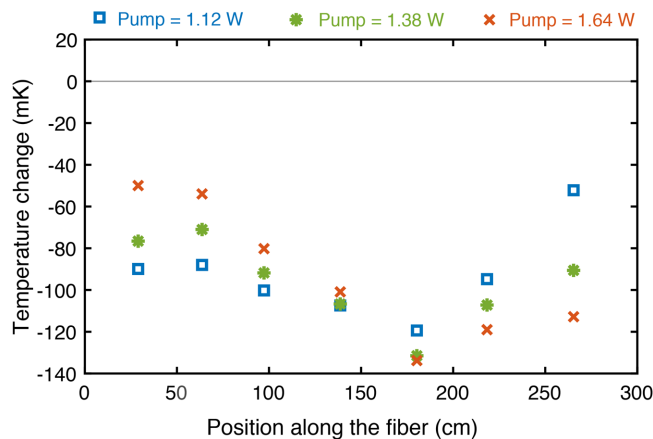


FIG. 3. Average temperature change ($n = 3$) measured at seven locations along a 2.74-m silica fiber amplifier for three pump powers at 1040 nm and a 3-mW seed at 1064 nm.

smaller near both ends, where the pump power is either above (at the input) or below (at the output) this optimum value (510 mW), and (ii) the lowest temperature is observed in the middle of the fiber, where the pump power is close to the optimum.

When the launched pump power was increased to 1.38 W, the signal output increased to 26 mW (a gain of 9.1 dB). As expected, the negative temperature change (green asterisks in Fig. 3) at the fiber input was now smaller than in the first case (blue squares), because the input pump power was further above the 510-mW optimum. This increase in launched power also resulted in a higher pump power at the fiber output end (154 mW). Since this value was now closer to the optimum, the output end of the fiber experienced a larger negative temperature change. The trend continued when the pump power was further increased to 1.64 W (red crosses): Cooling decreased near the input end and increased near the output end, where the residual pump power was now 247 mW. The signal amplification also increased, resulting in 11.4 dB of gain (44.6 mW of output power).

Figures 4(a)–4(c) plot the temperature data from Fig. 3 along with simulation results from the model of a radiation-balanced fiber laser described in Ref. [15] but with the cavity removed to simulate a fiber amplifier. For each temperature measurement, the standard deviation was calculated. The error bars in Fig. 4 represent the average of these values (± 6 mK). All the fiber parameter values needed for these simulations were either measured or inferred from fits to independent cooling and absorption measurements (see Supplemental Material [29]). Thanks to this comprehensive characterization, no fitting parameters were needed to generate the solid curves in Fig. 4. For each pump power, the measured temperatures agree well with simulations. From the model curves, the average temperature change is -107 mK for 1.12 W of input pump power, -105 mK for 1.38 W, and -93 mK for 1.64 W. The blue

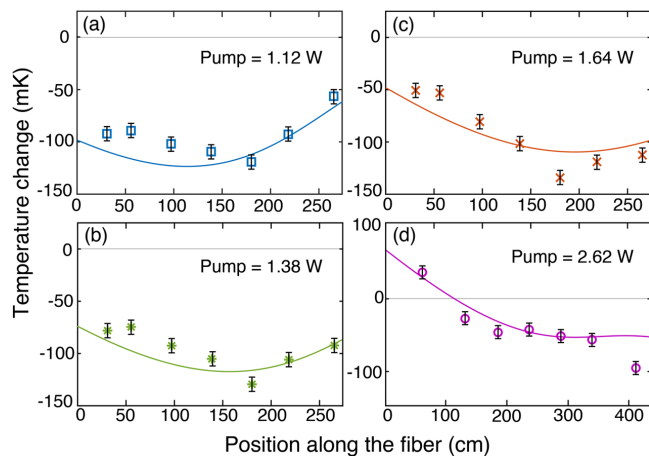


FIG. 4. Measured temperature change versus position along the fiber amplifier and simulated dependencies using the model based on Ref. [15] for (a)–(c) a 2.74-m and (d) a 4.35-m amplifier fiber.

curve in Fig. 5 shows the simulated average temperature change as a function of the input pump power. As expected, the cooling initially increases with pump power as more of the Yb ions are excited but eventually plateaus and starts to decrease as the cooling saturates and the additional power induces more heating (around 1.1 W).

To increase the gain, the pump power was increased to 2.62 W, and the length of the amplifier was increased to 4.35 m, the calculated optimum for this power. This resulted in 16.9 dB of gain (146 mW of output power at 1064 nm), while the average temperature change remained negative [see Fig. 4(d)]. The higher pump power resulted in a positive temperature change at the input end, but once the power was sufficiently attenuated (after ~ 100 cm) the fiber cooled below room temperature for the remaining length. The solid curve in Fig. 4(d) is the temperature profile predicted by the amplifier model. It is in excellent

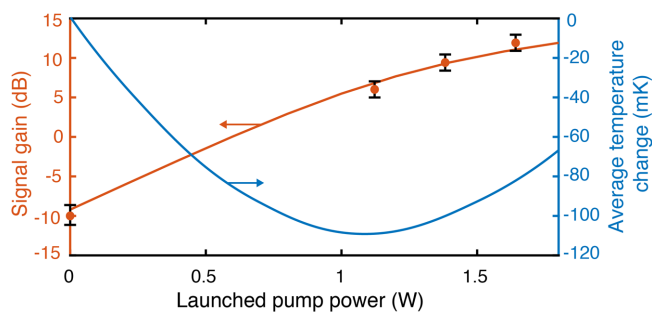


FIG. 5. Measured (red points) and simulated (red curve) small-signal gain at 1064 nm for a 3-mW seed as a function of the input pump power at 1040 nm into a 2.74-m silica fiber amplifier and the associated temperature change along the length of the amplifier as predicted by the model based on Ref. [15] (solid blue curve).

agreement with the measured temperature changes. The average temperature of the amplifier was -24.4 mK.

The gain of the 2.74-m amplifier was measured and plotted as a function of the input pump power (red points in Fig. 5). The error bars represent the measured standard deviation. The solid red curve was generated with the same model as above. The excellent fit confirms the accuracy of the model and of the measured and inferred parameter values for the Yb-doped silica fiber.

This work reports the first radiation-balanced fiber amplifier in a fiber made not of a fluoride glass but of silica, a significantly more ubiquitous, yet challenging material due to its historically low threshold for concentration quenching. The fiber used in this work has an aluminosilicate composition tailored to be doped with as much as 2500 ppm of Yb^{3+} while exhibiting negligible concentration quenching. The fiber was core pumped at 1040 nm to cool the core while amplifying a 3-mW seed at 1064 nm. With 2.62 W of launched pump power, the 4.35-m fiber amplifier produced 16.9 dB of small-signal gain while maintaining a negative average temperature of -24.4 mK below room temperature. To put this in perspective, the average temperature of a typical fiber amplifier pumped with 1 W at 976 nm is ~ 9 K above room temperature [5]. This work establishes that fiber technology is now capable, for the first time in history, to produce silica fibers with such chemical purity and low degree of quenching that they can be doped with unprecedented concentrations of ytterbium. In such a fiber, we showed that light can be coherently amplified with a gain approaching 20 dB and generate *no net internal heating*. This fundamental development is ushering silica fibers into a new era where it is possible to create fiber lasers and amplifiers with groundbreaking coherence and stability.

The authors thank Carston Langrock (Stanford University) for the generous amount of equipment he has lent to this project and Nanjie Yu for measuring the fiber's radiative lifetime. This work was supported by the Air Force Office of Scientific Research Grant No. FA9550-16-1-0383. See Supplemental Material [29] for supporting content.

*Jennyknall@stanford.edu

- [1] R. J. Mears, L. Reekie, S. B. Poole, and D. N. Payne, *Electron. Lett.* **21**, 738 (1985).
- [2] J. Geng, C. Spiegelberg, and S. Jiang, *Photonics Technol. Lett.* **17**, 1827 (2005).
- [3] <http://www.ipgphotonics.com/en/products/lasers/high-power-cw-fiber-lasers/1-micron/yfs-sm-1-10-kw>.
- [4] J. Y. Allain, M. Monerie, H. Poignant, and T. Georges, *J. Non-Cryst. Solids* **161**, 270 (1993).
- [5] M. K. Davis and M. J. F. Digonnet, *J. Lightwave Technol.* **16**, 1013 (1998).
- [6] N. A. Brilliant and K. Lagonik, *Opt. Lett.* **26**, 1669 (2001).
- [7] C. Jauregui, C. Stihler, and J. Limpert, *Adv. Opt. Photonics* **12**, 429 (2020).
- [8] S. Bowman, *IEEE J. Quantum Electron.* **35**, 115 (1999).
- [9] S. Bowman, S. P. O'Connor, S. Biswal, N. J. Condon, and A. Rosenberg, *IEEE J. Quantum Electron.* **46**, 1076 (2010).
- [10] R. Epstein and M. Sheik-Bahae, *Optical Refrigeration: Science and Applications of Laser Cooling of Solids* (Wiley-VCH, Weinheim, 2009).
- [11] P. C. Schultz, *J. Am. Ceram. Soc.* **57**, 309 (1974).
- [12] F. Auzel, G. Baldacchini, L. Laversenne, and G. Boulon, *Opt. Mater.* **24**, 103 (2003).
- [13] Z. Yang, J. Meng, A. R. Albrecht, and M. Sheik-Bahae, *Opt. Express* **27**, 1392 (2019).
- [14] J. Khurgin, *J. Opt. Soc. Am. B* **37**, 1886 (2020).
- [15] J. Knall and M. J. F. Digonnet, *J. Lightwave Technol.* **39**, 2497 (2021).
- [16] G. Nemova and R. Kashyap, *Proc. SPIE* **7686**, 768614 (2010).
- [17] X. Xia, A. Pant, E. J. Davis, and P. Pauzauskie, *J. Opt. Soc. Am. B* **36**, 3307 (2019).
- [18] G. Nemova and R. Kashyap, *J. Opt. Soc. Am. B* **26**, 2237 (2009).
- [19] E. Mobini, M. Peysokhan, and A. Mafi, *J. Opt. Soc. Am. B* **36**, 2167 (2019).
- [20] J. Knall, M. Esmaelpour, and M. J. F. Digonnet, *J. Lightwave Technol.* **36**, 4752 (2018).
- [21] R. I. Epstein, M. I. Buchwald, B. C. Edwards, T. R. Gosnell, and C. E. Mungan, *Nature (London)* **377**, 500 (1995).
- [22] T. R. Gosnell, *Opt. Lett.* **24**, 1041 (1999).
- [23] J. Knall, A. Arora, M. Bernier, S. Cozic, and M. J. F. Digonnet, *Opt. Lett.* **44**, 2338 (2019).
- [24] J. Knall, P. B. Vigneron, M. Engholm, P. Dragic, N. Yu, J. Ballato, M. Bernier, and M. J. F. Digonnet, *Opt. Lett.* **45**, 1092 (2020).
- [25] E. Mobini, S. Rostami, M. Peysokhan, A. Albrecht, S. Kuhn, S. Hein, C. Hupel, J. Nold, N. Haarlammert, T. Schreiber, R. Eberhardt, A. Tünnermann, M. Sheik-Bahae, and A. Mafi, *Commun. Phys.* **3**, 1 (2020).
- [26] J. Knall, M. Engholm, J. Ballato, P. Dragic, N. Yu, and M. J. F. Digonnet, *Opt. Lett.* **45**, 4020 (2020).
- [27] M. Peysokhan, S. Rostami, E. Mobini, A. Albrecht, S. Kuhn, S. Hein, C. Hupel, J. Nold, N. Haarlammert, T. Schreiber, R. Eberhardt, A. Tünnermann, M. Sheik-Bahae, and A. Mafi, [arXiv:2011.11224](https://arxiv.org/abs/2011.11224).
- [28] J. Ballato and P. Dragic, *J. Dir. Energy* **6**, 175 (2017).
- [29] See Supplemental Material at <http://link.aps.org/supplemental/10.1103/PhysRevLett.127.013903> for supporting content, which includes Refs. [30–32]
- [30] W. Krupke, *IEEE J. Quantum Electron.* **10**, 450 (1974).
- [31] S. R. Bowman and C. E. Mungan, *Appl. Phys. B* **71**, 807 (2000).
- [32] P. Barua, E. H. Sekiya, K. Saito, and A. J. Ikushima, *J. Non-Cryst. Solids* **354**, 4760 (2008).
- [33] A. Arora, M. Esmaelpour, M. Bernier, and M. J. F. Digonnet, *Opt. Lett.* **43**, 3337 (2018).